Pergamon

Int. J. Heat Mass Transfer. Vol. 41, No. 2, pp. 447–464, 1998

Printed in Great Britain
0017–9310/98 $19.00+0.00

PII: S0017-9310(97)00133-6

Experimental studies and numerical simulation of evaporative cooling of air with a water spray—I. Horizontal parallel flow

S. S. KACHHWAHA,† P. L. DHAR and S. R. KALE‡

Mechanical Engineering Department, Indian Institute of Technology, Hauz Khas, New Delhi-110016, India

(*Received* 13 *January* 1997)

Abstract—Hollow cone water sprays are used in many humidifying, cooling and scrubbing applications. For predicting the heat and mass transfer in these spray–air flow systems a two-dimensional numerical model simulating the conservation of mass, momentum and energy of air, and water, were developed. Model inputs include drop size distribution and velocities at nozzle spray angle; inlet air DBT and humidity ratio. The set of conservation equations are time marched numerically and conditions at various downstream locations are computed. Experimental data were obtained on a horizontal once through wind tunnel at three air velocities with each nozzle at three pressures in parallel flow configuration. Nozzles of 3.2 and 4.8 mm outlet diameter were used. Drop diameter at break-up was measured from still photographs of the spray and these data were used in the model. Predictions of air condition at wind tunnel outlet for given input conditions agree well with experimental data. © 1997 Elsevier Science Ltd.

1. INTRODUCTION

Water sprays are extensively used in several engineering applications, such as, dust control, fire fighting, nuclear reactor core cooling, spray drying, air scrubbing and evaporative cooling. In hot and dry climates, such as the summer season in India and other parts of the world, evaporative cooling of air is an attractive energy efficient technique for producing a comfortable indoor environment. Air washers employed in large air-conditioning systems for dust removal can also be optimized for evaporative cooling with appropriate design modifications which can result in energy savings.

In typical air washers, pressurized water is admitted into nozzles arranged in an array, from where it emerges as a thin bell-shaped hollow cone which disintegrates into polydisperse drops moving at different velocities. After travelling through the air most drops fall to the floor and some drops drift with the air. This drop motion in air causes heat and mass transfer due to evaporation and some sensible cooling. In this complex multiphase, three-dimensional system, an understanding of the dynamics of drop–air interaction is crucial for optimizing the process.

2. LITERATURE REVIEW

The study of water spray–air interaction involves several fields of engineering, namely, fluid dynamics, sprays, heat and mass transfer and multiphase dynamics which are encountered in a vast range of applications listed above. The literature on sprays and heat and mass transfer is, consequently, distributed across several disciplines. Given below is a concise description of literature directly applicable to the present work.

2.1. *Heat and mass transfer*

The analysis of gas–drop systems involves solving the mass, momentum and energy conservation equations for each phase. This coupled phenomenon is very complex because of turbulence, cloud-like behaviour and non-linear variation due to properties. Industrial designers have, for a long time, based their designs on empirical analyses and a summary of these is given by Masters [1].

In some applications, the air/gas flow field is not affected or weakly affected by the presence of drops. The problem then reduces to calculating drop trajectories and their temperature history through the assumed flow field. In dispersed flow, the drop phase conservation equations can be described either by Lagrangian or Eulerian formulation and both have been used in the past. Various equations involved in Lagrangian motion analysis are mentioned in Yeung [2], and Crowe *et al.* [3]. The drawback of the Eulerian formulation is that it consists of a system of partial differential equations, which makes it mathematically unattractive as compared to the Lagrangian formulation which involves only ordinary differential equations.

Numerical solutions of the governing equations of

† Present Address: Department of Mechanical Engineering, Engineering College, Kota-324 010, India.

‡ Author to whom correspondence should be addressed.

NOMENCLATURE

A	cross-section area of the test section
A_s	surface area of drop
a	dimensionless parameter
a_i	Lagrangian constants ($i = 0, 1, 2, 3$)
C_d	coefficient of drag
C_f	coefficient of friction for flat plate
$C_{p,av}$	average specific heat of air
C_{pd}	specific heat of drop
C_v	coefficient of velocity
D	drop diameter
D_{30}	volume mean diameter
D_h	hydraulic diameter
DBT	dry bulb temperature
$\mathscr{D}$	diffusivity coefficient of water vapour in air
D_{max}	maximum drop diameter
D_{min}	minimum drop diameter
$\bar{D}_{max}$	normalized maximum drop diameter
$\bar{D}_{min}$	normalized minimum drop diameter
$\bar{D}$	dimensionless drop diameter
f	joint drop size and velocity distribution function
f_f	friction factor
g	constant for gravity
h	heat transfer coefficient
h_a	enthalpy of air
h_d	enthalpy of drop
h_{fg}	enthalpy of evaporation
$h_{fg,wall}$	enthalpy of evaporation at duct wall temperature
$h_{fg,0}$	enthalpy of evaporation at 0°C
h_m	mass transfer coefficient
$h_{m,wall}$	mass transfer coefficient of inner duct wall
h_{wall}	heat transfer coefficient of inner duct wall
k_a	thermal conductivity of air
L	duct length
m	mass flow rate of air
N	number of drops per second
n	number of drops per second per unit cross-section area of duct
Nu	Nusselt number
Nu_D	Nusselt number based on hydraulic diameter
P	duct perimeter
Pr	Prandtl number
p_{vs}	saturation pressure corresponding to air
p	pressure at the cross-section of the duct
Δp	pressure difference across the nozzle
Q_{act}	actual nozzle discharge
Re_D	duct Reynolds number
Re_d	drop Reynolds number
RH	relative humidity in percentage
Sc	Schmidt number
Sh	Sherwood number
Sh_D	Sherwood number based on hydraulic diameter
$\bar{S}_e$	dimensionless energy source term
$\bar{S}_m$	dimensionless mass source term
$\bar{S}_{mv}$	dimensionless momentum source term
T_a	air temperature
$T_{a,in}$	temperature of air at drift eliminator inlet
T_d	drop temperature
$T_{s,de}$	surface temperature of drift eliminator
T	water temperature
T_{wall}	temperature of duct wall surface
t	time
U	drop velocity
u_0	nozzle velocity
U_{max}	maximum drop velocity
U_{min}	minimum drop velocity
$\bar{U}_{max}$	dimensionless maximum drop velocity
$\bar{U}_{min}$	dimensionless minimum drop velocity
$\bar{U}$	dimensionless drop velocity
U_x	drop velocity in x-direction
U_y	drop velocity in y-direction
u	air velocity inside the duct
W	relative velocity of drop w.r.t. air
We	Weber number of drop
X	mass fraction of water vapour
X_s	mass fraction of water vapour at the drop surface
X_{wall}	mass fraction of water vapour at the surface of duct wall
x	positive direction along the duct.

Greek letters

σ	surface tension
ρ_a	density of air
ρ_l	density of water
μ_a	absolute viscosity of air
λ	ratio of air to vapour molecular weight
ω	humidity ratio
ϕ	relative humidity
ν_a	kinetic viscosity of air.

Subscripts

a	air
act	actual
av	average condition
D	drag
d	drop
e	energy transfer condition, exit
fg	evaporation
i	general designation, drop volume space
in	inlet
l	liquid condition

NOMENCLATURE (continued)

Subscripts

m	mass transfer condition	s	surface, saturation condition
max	maximum	v	vapour
min	minimum	vs	saturation condition of vapour
mv	momentum transfer condition	wall	duct wall condition
o	nozzle outlet condition	x	coordinate
out	outlet	y	coordinate
p	constant pressure condition	0	zero Celsius
		30	volume mean.

gas–liquid spray systems can be obtained by finite difference methods. The domain of interest is divided into a finite number of computational cells or grids and gas and liquid phase equations are separately represented in a finite difference technique over each cell. This process finally results in a system of algebraic equations, usually linearized, relating the unknowns of each computational cell. These equations are then solved to give the flow field of each phase simultaneously. A detailed description of such a numerical procedure is given in Harlow and Amsden [4]. The particle source-in-cell model, Crowe *et al.* [3] solves the gas and flow fields iteratively. The drop field is treated as sources of mass and momentum for the gas field in each computational cell. This technique has been extended to gas–liquid systems where heat and mass transfer also occur. A simple numerical model of a water spray humidifier was developed by Hiestand *et al.* [5]. In this analysis, a set of one-dimensional, ordinary differential equations based on conservation principles was developed and numerically solved to model the streamwise behaviour of hot flue gas and water drops in a humidification process for sulfur emission control. A similar simulation of hollow cone spray and air interaction was developed by Kachhwaha *et al.* [6], which was later extended to two-dimensional in Kachhwaha *et al.* [7]. An integral analysis was proposed by Yeung [2] for the case of negligible mass transfer and incompressible gas phase. Yeung [8] also presented a similarity analysis of gas–liquid spray systems (conical and flat spray) based on a simplified set of governing equations.

Several studies conducted for predicting the detailed flow and thermal characteristics of spray units especially in fire fighting applications are described by Mawhinney *et al.* [9]. Mohiuddin and Kant [10] presented a review on the analysis of mechanical-draft wet cooling towers and compared different numerical models from the view point of design, computational error, computational time, simplicity of usage and practicability. A three-dimensional model has been given by Palaszewski *et al.* [11] using which they computed the local variation in the dry bulb temperature, absolute humidity and air streamlines throughout the flow field and their effect on local variation of drop cooling. They treated the conservation equations as spatially varying sources of mass, momentum and energy, and used correlations for local drop heat and mass transfer coefficients and turbulent mixing models for the air vapour phase to close the set of equations. Palaszewski *et al.* [12] used this model for the design, performance prediction and improvement of spray units for power plant spray cooling ponds. Moussiopoulous and Ernst [13] and Moussiopoulous [14] developed a numerical model for predicting the thermal performance of a circular spray cooling pond in the case of zero wind velocity. The air flow is described by partial differential equations for the vorticity and stream function. Turbulence is taken into account by a modified version of the k–ε model. Temperature and humidity are obtained by solving appropriate transport differential equations. This system of equations was solved by a finite difference method and their results were in good agreement with experimental observations.

A study of one- and two-dimensional water sprays in air was performed by Ghosh and Hunt [15]. They analytically calculated spray induced air velocity field for a spray emerging into a quiescent environment. They show that a two-dimensional fan spray and a one-dimensional axisymetric spray can be modelled mathematically as a line source of momentum due to which surrounding air behind the jet is sucked towards the spray centre line. This behaviour was also observed by Abhishek [16] for a hollow cone water spray in his flow visualization experiments. In a companion paper Ghosh and Hunt [17] calculated the induced air velocity for the same sprays in the presence of a cross wind. They did not study parallel and counter flow configurations and their focus was limited to momentum exchange in a non-evaporating spray–gas system environment. Apart from these studies, there has been considerable research related to combustion, spray drying and fire fighting, amongst others, where large temperature gradients occur. There are, however, very few studies related to the topic of the present work where temperature difference is small and evaporation is the primary heat-mass transfer mode.

2.2. *Spray characterization*

An important input to the heat and mass transfer models is the spray characteristics quantified by drop diameter and velocity distribution at an appropriate

location in the flow. This information is highly nozzle specific and due to the complex nature, very difficult to quantify. The advent of non-intrusive techniques based on lasers has enabled collection of such data, as described by Hishida *et al.* [18], Maeda *et al.* [19, 20], Sellens [21], Li *et al.* [22], Azzopardi [23], and Natrajan [24]. Such methods besides being expensive still fall short of the extent of details which are required in heat and mass transfer models. Analytically, a variety of techniques have been used to mathematically described the drop diameter–velocity distribution produced at the origin of the spray. Mugele and Evans [25] reviewed the various distribution functions, such as, Rosin and Rammler, Nukiyama and Tanasawa and log probability in regard to their theoretical soundness and application to spray data. They proposed a new equation, called the upper-limit equation, as a standard for describing drop size distributions in sprays. This equation, based on the differential equation of the normal or Gaussian distribution, is

$$y = \ln\{aD/(D_{\max} - D)\} \tag{1}$$

where, a is a dimensionless parameter, D is drop diameter and $D_{\max}$ is the maximum stable drop diameter. The upper limit equation has been successfully applied to a wide variety of experimental data on sprays. Lekic *et al.* [26] compared the upper-limit function and chi-square distribution and concluded that the determination of the best estimates of the parameters for upper limit function is easier and the convergence is faster than in the case of the chi square distribution. Lee and Tankin [27] used upper limit distribution for simulation of hollow cone spray. One of the most promising approaches is based on the use of the maximum entropy principle developed by Jaynes [28] from Shannon's [29] concept of entropy. This approach has now been developed into the generalized maximum entropy principle [30, 31], which states that the most appropriate probability distribution is the one which maximizes Shannon's entropy subject to the given constraints imposed upon a physical probabilistic system (or process). For sprays, the most probable drop size and velocity distribution can be obtained by maximizing Shannon's entropy under the constraints of the partial information known about the atomization process, i.e. the conservation laws. Sellens and Brzustowski [32], and Sellens [33] used this technique where they assumed that the direct kinetic energy and surface energy are separately conserved during the break-up process of the liquid sheet, along with the conservation of liquid mass and momentum during the same processes. Li and Tankin [34] derived an expression for the joint drop size and velocity distribution using the MEP and the physical conservation laws of mass, momentum and total energy (the sum of direct kinetic energy and surface energy). The expression for conservation of energy results in an explicit dependence of the PDF on the Weber number. The constraints imposed on liquid atomization are conservation of mass, momentum, and total energy (the sum of kinetic energy and surface energy). In addition there is the requirement that the sum of the joint probabilities be unity. On non-dimensionalization, this gives:

mass conservation

$$\int_{\bar{D}_{\min}}^{\bar{D}_{\max}} \int_{\bar{U}_{\min}}^{\bar{U}_{\max}} f\bar{D}^3 \,\mathrm{d}\bar{U}\,\mathrm{d}\bar{D} = 1 + \bar{S}_{\mathrm{m}} \tag{2}$$

momentum conservation

$$\int_{\bar{D}_{\min}}^{\bar{D}_{\max}} \int_{\bar{U}_{\min}}^{\bar{U}_{\max}} f\bar{D}^3 \bar{U}\,\mathrm{d}\bar{U}\,\mathrm{d}\bar{D} = 1 + \bar{S}_{\mathrm{mv}} \tag{3}$$

energy conservation

$$\int_{\bar{D}_{\min}}^{\bar{D}_{\max}} \int_{\bar{U}_{\min}}^{\bar{U}_{\max}} f(\bar{D}^3 \bar{U}^2 + B\bar{D}^2)\,\mathrm{d}\bar{U}\,\mathrm{d}\bar{D} = 1 + \bar{S}_{\mathrm{e}} \tag{4}$$

normalization

$$\int_{\bar{D}_{\min}}^{\bar{D}_{\max}} \int_{\bar{U}_{\min}}^{\bar{U}_{\min}} f\,\mathrm{d}\bar{U}\,\mathrm{d}\bar{D} = 1 \tag{5}$$

Here $\bar{S}_{\mathrm{m}}$, $\bar{S}_{\mathrm{mv}}$, $\bar{S}_{\mathrm{e}}$ are the non-dimensional mass, momentum and energy source terms, respectively, and 'f' is the joint drop size and velocity distribution function which maximizes Shannon's entropy subject to the constraints of equations (2)–(5). Thus, 'f' can be shown to have the following form [34]:

$$f = 3\bar{D}^2 \exp\{-a_0 - a_1\bar{D}^3 - a_2\bar{D}^3\bar{U} - a_3(\bar{D}^3\bar{U}^2 + B\bar{D}^2)\} \tag{6}$$

where $\bar{D} = D/D_{30}$ is the dimensionless drop diameter, $\bar{U} = U/U_0$ is the dimensionless drop velocity, $B = 12/We$; a_0, a_1, a_2 and a_3 are Lagrangian multipliers, and Weber number $We = \rho_1 U_0^2 D_{30}/\sigma$. Equation (6) shows that for any particular drop size, the velocity distribution is Gaussian. The system of equations governing the distribution function, equations (2)–(5), are highly non-linear for which no analytical solution exists and a numerical procedure must be implemented. As shown by Li *et al.* [35], the solution not only exists, but is unique as well, provided that each source term in equations (2)–(4) takes value between -1 and infinity.

The drop number-based size distribution (or more frequently called drop number distribution) can be determined by integrating equation (6) over the velocity space from minimum to maximum velocity. Thus, the drop number distribution, which is usually denoted by $\mathrm{d}N/\mathrm{d}\bar{D}$, becomes

$$\frac{\mathrm{d}N}{\mathrm{d}\bar{D}} = \int_{\bar{U}_{\min}}^{\bar{U}_{\max}} f\,\mathrm{d}\bar{U} = \frac{3}{2}\left(\frac{\bar{D}}{a_3}\right)^{1/2} [\mathrm{erf}(X_{\max}) - \mathrm{erf}(X_{\min})] \times \exp\left[-a_0 - a_3 B\bar{D}^3 - \left(a_1 - \frac{a_2^2}{4a_3}\right)\bar{D}^3\right] \tag{7}$$

where erf(X) denotes the error function, N the normalized cumulative drop number, and

$$X_{\max} = \left(\bar{U}_{\max} + \frac{a_2}{2a_3}\right)(a_3\bar{D}^3)^{1/2} \tag{8a}$$

$$X_{\min} = \left(\bar{U}_{\min} + \frac{a_2}{2a_3}\right)(a_3\bar{D}^3)^{1/2}. \tag{8b}$$

Likewise, the number-based drop velocity distribution, $dN/d\bar{U}$, can be obtained by integrating equation (6) over the drop size space from the minimum to maximum drop diameter:

$$\frac{dN}{d\bar{U}} = \int_{\bar{D}_{\min}}^{\bar{D}_{\max}} f\, d\bar{D}. \tag{9}$$

The above integration can be performed numerically using maximum and minimum values of dimensionless drop diameter from zero to infinity; and dimensionless drop velocity between 0 and 2.0, 0.5 and 1.5, 0 and ∞ and 0-stability limit. Using the above procedure, the joint PDF for an atomizing spray can be determined. The inputs required for the solution of the above system of equations are maximum and minimum values of drop diameter and velocity, nozzle exit velocity, volume mean diameter and source terms.

Li and Tankin [34] obtained the Lagrangian multiplier by solving the constraints equations by a modified Newton–Raphson method. They obtained a set of Lagrangian multipliers that yielded $\bar{S}_m = \bar{S}_e = 0$, $\bar{S}_{mv} = -0.05$. The selected values for $\bar{U}_{\min}$ and $\bar{U}_{\max}$, based on the experimental measurement were 0.5 and 1.5, respectively. Li *et al.* [22] made a comparison between experiments and predictions based on MEP for sprays of a pressure atomizer. The agreement between the measurements and the prediction was satisfactory. Thus, the MEP formalism has the potential for providing the joint drop diameter and velocity distribution function from minimal experimental data on drop diameter or velocity and hence, this was used in the present work.

3. HEAT AND MASS TRANSFER MODEL

3.1. *The approach*

The heat and mass transfer model was adopted for drop diameter and velocity data from the MEP formalism. For using the latter, sprays were produced in quiescent air, and photographs were taken at break-up. These pictures were analyzed manually for obtaining drop diameter distribution from which the volume mean diameter was calculated. This data along with calculated liquid sheet velocity at break-up was input to the MEP formalism and the joint drop diameter and velocity distribution was obtained. This continuous function was discretized into five drop diameter ranges (referred to as categories) with a unique velocity assigned to each based on MEP formalism at the sheet break-up point. The conservation equations were then applied to each drop category individually which were then summed up for the five categories to obtain the complete behaviour at a given location. A description of the conservation equation used in this analysis is given below.

3.2. *Model development*

In the present model, the three-dimensional axisymmetric spray originating into a $0.6 \times 0.6 \times 2$ m long wind tunnel has been modelled as a planar two-dimensional system with drops originating at two angles (Fig. 1), which interact with a uniform one-dimensional laminar flow in parallel configuration. This geometry has been adopted for all the simulations. Half the drops are modelled as being ejected above the spray centreline and the other half below it. Some drops hit the tunnel walls and are removed from the simulation and some others attain free stream velocity and are carried by air, i.e. drift. The drop size distribution at break-up was obtained by the maximum entropy formalism [22] details of which are given in Section 2.2. For simplicity and ease of simulation, these drops have been re-distributed in five distinct diameter categories, each characterized by its mean diameter and a mean velocity.

Figure 1 also shows the control volume for analysis. As the flow proceeds downstream, perfect transverse mixing is assumed at each location. Thus, heat and mass transfer from a drop in the control volume is assumed to spread immediately and uniformly everywhere in the control volume (see Fig. 1). The duct wall is assumed to be adiabatic, but heat and mass transfer due to evaporation from wet walls is included in the model. The duct pressure is assumed to be constant and equal to the ambient pressure as a result of which momentum transfer between drops and air is neglected. This assumption simplifies the computations considerably without any major effect on heat and mass transfer calculations. Finally, at the wind tunnel exit, a drift eliminator was provided to remove the drifting water drops; its surfaces were wet and hence, their contribution to air cooling has also been included.

3.3. *Conservation equations*

The mass, momentum and energy conservation equations which comprise the model, are described below.

3.3.1. *Conservation of mass.* The conservation of water vapour mass in air can be expressed as under where the increase in mass and mass fraction of water in the air water mixture (X) occurs due to evaporation of drops, wet tunnel surfaces and wet surfaces of the drift eliminator.

$$\frac{dX}{dx} = \sum_i \frac{n_i h_{m,i} A_{s,i}(X_{s,i} - X)}{U_{x,i} u} + \frac{h_{m,\text{wall}} P \cdot (X_{\text{wall}} - X)}{Au} - \frac{X}{u}\frac{du}{dx} - \frac{X}{\rho_a}\cdot\frac{d\rho_a}{dx}. \tag{10a}$$

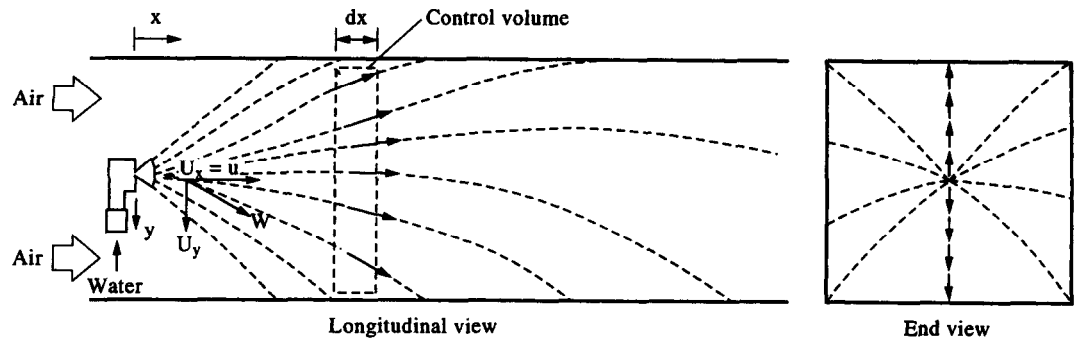

Fig. 1. System for flow modelling.

Similarly conservation of mass for air can be written as:

$$\rho_a(1-X)uA = \text{Constant.} \tag{10b}$$

The drop evaporation causes mass loss which is reflected in their decreasing diameters. For drops of category "i", the conservation of drop mass can be written as:

$$\frac{dD_i}{dx} = \frac{h_{m,i}\rho_a(X_{s,i}-X)}{\rho_l U_{x,i}}. \tag{10c}$$

3.3.2. *Conservation of momentum.* For air, the conservation of x-momentum represents the balance of air acceleration with momentum addition from drops, change of mass (due to evaporation from drops), pressure gradient in duct and wall shear stresses [36]. In the present model air pressure in the wind tunnel was assumed constant throughout the duct. Momentum exchange between air and drops has also been assumed to be negligible and, therefore, the air momentum equation is not used in the simulations.

The deceleration of "i" category drops in x-direction can be expressed as follows:

$$\frac{dU_{x,i}}{dx} = -\frac{0.75C_{D,i}\rho_a W_i(U_{x,i}-u)}{U_{x,i}\rho_l D_i} - \frac{3U_{x,i}}{D_i}\frac{dD_i}{dx}. \tag{11a}$$

Here, the right-hand side represents drag force and inertia forces occurring due to changing drop mass. For y-momentum, the deceleration is balanced by buoyancy in addition to the two terms appearing on the right-hand side of equation (11a).

$$\frac{dU_{y,i}}{dx} = \frac{g(\rho_l-\rho_a)}{U_{x,i}\rho_l} - \frac{0.75C_{D,i}\rho_a W_i U_{y,i}}{\rho_l D_i U_{x,i}} - \frac{3U_{y,i}}{D_i}\frac{dD_i}{dx}. \tag{11b}$$

Drop trajectories can also be expressed in terms of coordinates and X- and Y-velocity components by

$$\frac{dy_i}{dx} = \frac{U_{y,i}}{U_{x,i}}. \tag{11c}$$

3.3.3. *Conservation of energy.* Change in air temperature occurs due to mass and heat transfer from drops and from the walls which can be expressed as follows:

$$\frac{dT_a}{dx} = \sum_i \frac{[n_i h_{fg,i}\pi D_i^2 h_{m,i}\rho_a(X_{s,i}-X) - n_i h_i \pi D_i^2(T_a-T_d)]}{C_{p,av}\rho_a u U_{x,i}} + [h_{fg,wall}h_{m,wall}\rho_a(X_{wall}-X) - h_{wall}(T_a-T_{wall})]\left[\frac{P}{C_{p,av}\rho_a uA}\right] - \frac{h_a}{C_{p,av}}\left[\frac{1}{u}\frac{du}{dx}+\frac{1}{\rho_a}\frac{d\rho_a}{dx}\right] - \frac{h_{fg,0}}{C_{p,av}}\frac{dX}{dx}. \tag{12a}$$

Energy balance on ith category of drops represents the rate of change of drop temperature, and the mass and heat transfer occurring with air.

$$\frac{dT_{d,i}}{dx} = \frac{6[h_i(T_a-T_{d,i}) - h_{fg}h_{mi}\rho_a(X_{s,i}-X)]}{D_i\rho_l U_{x,i}C_{pd,i}} - \frac{3h_{d,i}}{C_{pd,i}D_i}\frac{dD_i}{dx}. \tag{12b}$$

3.4. *Correlations used*

3.4.1. *Drag coefficient.* Here each drop is assumed to behave like a rigid sphere for which drag coefficient-Reynolds number relations are available. For ease of computation, the correlations of Lin *et al.* [37] have been used:

$$C_D = 24/Re_d \quad \text{for } Re_d < 2 \tag{13a}$$

$$C_D = 18.197/Re_d^{0.599} \quad \text{for } 2 < Re_d < 500 \tag{13b}$$

and

$$C_D = 0.44 \quad \text{for } 500 < Re_d < 2\times 10^5. \tag{13c}$$

Here, Re_d is the drop diameter Reynolds number based on velocity of drops relative to the air which is expressed as:

$$Re_d = \frac{\rho_a W D}{\mu_a} \tag{14}$$

$$W = [(U_x - u)^2 + U_y^2]^{1/2}. \tag{15}$$

3.4.2. *Mass concentration properties.* The mass concentration of water vapour at the drop surface is given by:

$$X_s = \frac{p_{vs}}{\lambda p - (1-\lambda)p_{vs}} \tag{16}$$

where, λ is the ratio of the air to vapour molecular weight, p_{vs} the partial pressure of water vapour and p the total atmospheric pressure. For air water vapour mixture, λ is equal to 1.608. In general, p_{vs} can be approximated by the saturation pressure corresponding to the drop temperature.

The mass fraction of water vapour in air can be expressed as:

$$X = \frac{\omega}{1+\omega} \tag{17}$$

where, ω is humidity ratio, which is related to the saturation pressure, p_{vs}, and relative humidity, ϕ, at the drop temperature by the following expression [38].

$$\omega = \frac{0.62198 FS(T)\phi p_{vs}}{p - FS(T)\phi p_{vs}} \tag{18}$$

where

$p = 101325.0$ N/m^2
$FS(T) = 1.0046$ for $T \geqslant 0.0$
$FS(T) = 1.0044$ for $T \geqslant 4.0$
$FS(T) = 1.0044 - 0.0002/\{11(T\text{-}16)\}$ for $T > 16.0$
$FS(T) = 1.0046 + 0.0004/\{11(T\text{-}27)\}$ for $T > 27.0$
$FS(T) = 1.0046 + 0.0004/\{11(T\text{-}33)\}$ for $T > 38.0$.

Temperature T is in °C. Saturation pressure of water, p_{vs}, corresponding to temperature, T is given by

$$\begin{aligned} p_{vs} = \exp[&-5800.2206/T \\ &+ 1.3914993 - 0.048640239T \\ &+ 0.41764768 * 10^{-4} T^2 \\ &- 0.14452093 * 10^{-7} T^3 \\ &+ 6.5459673 \log T]. \end{aligned} \tag{19}$$

3.4.3. *Heat and mass transfer correlations.* The heat and mass transfer coefficient for drops have been determined from the correlations developed by Ranz and Marshall [39]:

$$Sh = \frac{h_m D}{\mathscr{D}} = 2.0 + 0.6 Re_d^{0.5} Sc^{0.33} \tag{20}$$

$$Nu = \frac{hD}{k_a} = 2.0 + 0.6 Re_d^{0.5} Pr^{0.33} \tag{21}$$

where, Sc is the Schmidt number

$$Sc = \frac{\mu_a}{\rho_a \mathscr{D}} \tag{22}$$

and, Pr is the Prandtl number

$$Pr = C_{p,av} \frac{\mu_a}{k_a} \tag{23}$$

where, μ_a and k_a are dynamic viscosity and thermal conductivity of air at temperature, T_a, and have been determined from the property data given by Dewitt and Incropera [40].

The mass diffusivity of water vapour in air, $\mathscr{D}$, has been estimated from the relation developed by Bird *et al.* [41]:

$$\mathscr{D} = 2.495 x 10^{-5} \left(\frac{T_a}{292.88}\right)^{2.334}. \tag{24}$$

3.4.4. *Specific heat of air and water.* Using the tabular property data given by [40], the property equations were developed for specific heat of water, vapour, air and specific enthalpy evaporation of water.

3.5. *Effect of drift eliminator*

The surfaces of the drift eliminator capture the drifting drops and are, consequently, wet; its surface temperature can, therefore, be assumed to be same as the drop temperature. While passing through the drift eliminator, the air is, therefore, cooled by sensible and evaporative cooling. The drift eliminator geometry has been modelled as a rectangular channel formed by two consecutive parallel drift eliminator plates. The plates are assumed to be straight (19.5 cm length × 64 cm height) in the flow direction with 3.6 cm spacing between them. Therefore, the cross-sectional area of this duct is 3.6 × 64 cm, and, the hydraulic diameter is:

$$D_h = 4 \frac{\text{cross-section area}}{\text{Perimeter}}. \tag{25}$$

The Reynolds number based on this dimension is:

$$Re_D = \frac{D_h u}{\nu_a}. \tag{26}$$

The Nusselt number based on hydraulic diameter can be calculated using the expression given by Gnielinski [42].

$$Nu_D = \frac{(f_f/8)(Re_D - 1000)Pr}{1 + 12.7(f_f/8)^{1/2}(Pr^{2/3} - 1)} \left[1 + \left(\frac{D_h}{L}\right)^{2/3}\right] \tag{27}$$

for $0.5 < Pr < 2000$ and $2300 < Re_D < 5 \times 10^6$, where, the friction factor is given by

$$f_f = (0.79 \ln Re_D - 1.64)^{-2}. \tag{28}$$

The Sherwood number based on hydraulic diameter is calculated according to the Gilliland correlation [41] for $Re_D > 2000$:

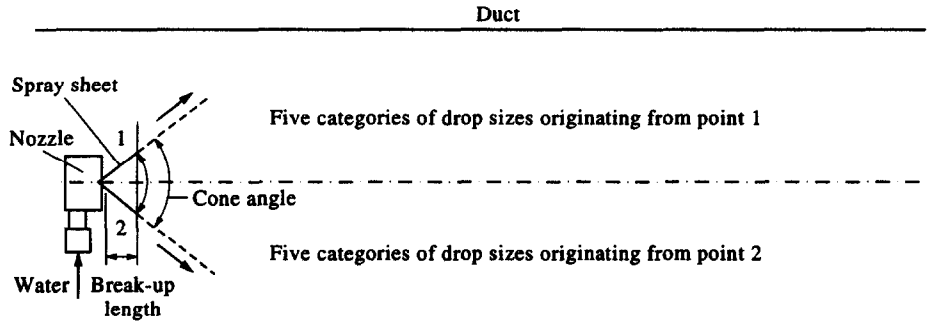

Fig. 2. Spray configuration used in solution technique.

$$Sh_D = 0.023 Re_D^{0.83} Sc^{0.44}. \quad (29)$$

Finally, for this type of configuration, axial variation of mean air temperature, $T_a(x)$, can be estimated by the following analytical expression [40]:

$$\frac{T_{s,de} - T_a(x)}{T_{s,de} - T_{a,in}} = \exp\left[-\frac{Px}{mC_{p,av}} h_{wall}\right] \quad (30)$$

where, $T_{s,de}$ is surface temperature of drift eliminator.

3.6. *Boundary conditions*

The simulations have been performed for steady state and the various boundary conditions which are representative of the experimental conditions (described later). The duct dimensions were $0.6 \times 0.6 \times 2$ m (long). The air velocity and temperature as measured at duct inlet during the experiments were used for simulations. The simulations have been performed for two nozzle diameters namely, 3.2 and 4.8 mm, each operating at water supply pressures of 1, 2 and 3 bar(g). Drop size and velocity distribution for five discrete drop diameters were obtained as mentioned in Section 4.1. Spray angle and water temperature were same as measured during experiments. Location of spray origin points (Fig. 2) were calculated from the break-up length and spray angle. During computations, if the drop y-coordinate attained a value of 0.3 m, i.e. half the duct height, then further calculation were stopped as the drop hits the duct wall. The detailed boundary conditions used a model inputs and the outputs of the simulations are shown in Fig. 3.

3.7. *Simulation procedures*

A total of 52 ordinary differential equations describe the air–water interaction: two for conservation of air mass and energy, 10 each for conservation of drop mass, energy and momentum in two different directions; and 10 for drop trajectory of each of the five drop diameter categories in the two halves of the duct. In addition, the correlations described in Sections 3.4 are also used.

4. EXPERIMENTAL SETUP

The experiments were conducted in two phases with two nozzles in each: first, for characterizing the spray and second, for determining the heat and mass transfer in a wind tunnel. The nozzles of outlet diameter 3.2 and 4.8 mm were used and their construction features are shown in Fig. 4.

4.1. *Spray characterization*

Each nozzle was individually supplied with pressurized water at 1, 2 and 3 bar(g) from a tank and pump system; it discharged into ambient air and the drops fell to the ground. At each supply pressure, the nozzle discharge was measured with a graduated cylinder. From the nozzle pressure, the nozzle velocity was calculated using the expression:

$$U_0 = C_v \left(\frac{2\Delta p}{\rho_l}\right)^{0.5} \quad (31)$$

where ρ_l is the density of water and, C_v is the coefficient of velocity of the nozzle (taken as 0.9). Photographs of the spray were used for measuring spray angles which were 64 and 76° for the 3.2 and 4.8 mm diameter nozzles, respectively. At the break up of the liquid sheet a high speed still camera was used to photograph the drops. At each pressure, four frames were analysed yielding an in-focus drop count in the range from 9700 to 16 300. For this purpose, the pictures were projected on a wall and drop diameters were measured manually in discrete ranges, each of 0.5 mm; with magnification of 5 and 8 (frame dependent), these yielded actual drop diameter resolution in steps of 100 and 62.5 μm, respectively. From this drop diameter distribution, the volume mean diameter D_{30} was calculated. These data were then used in the MEP formulation. This information also require values of the source terms for mass, momentum and energy. These were based on the technique given by Li *et al.* [22]. At ambient pressure and temperature, there is negligible variation in the water mass from nozzle outlet to spray formation due to evaporation (of the order of 10^{-4}) and, hence, the mass source term, $\bar{S}_m$, has been taken as zero. The energy source term, $\bar{S}_e$, consists of kinetic and surface

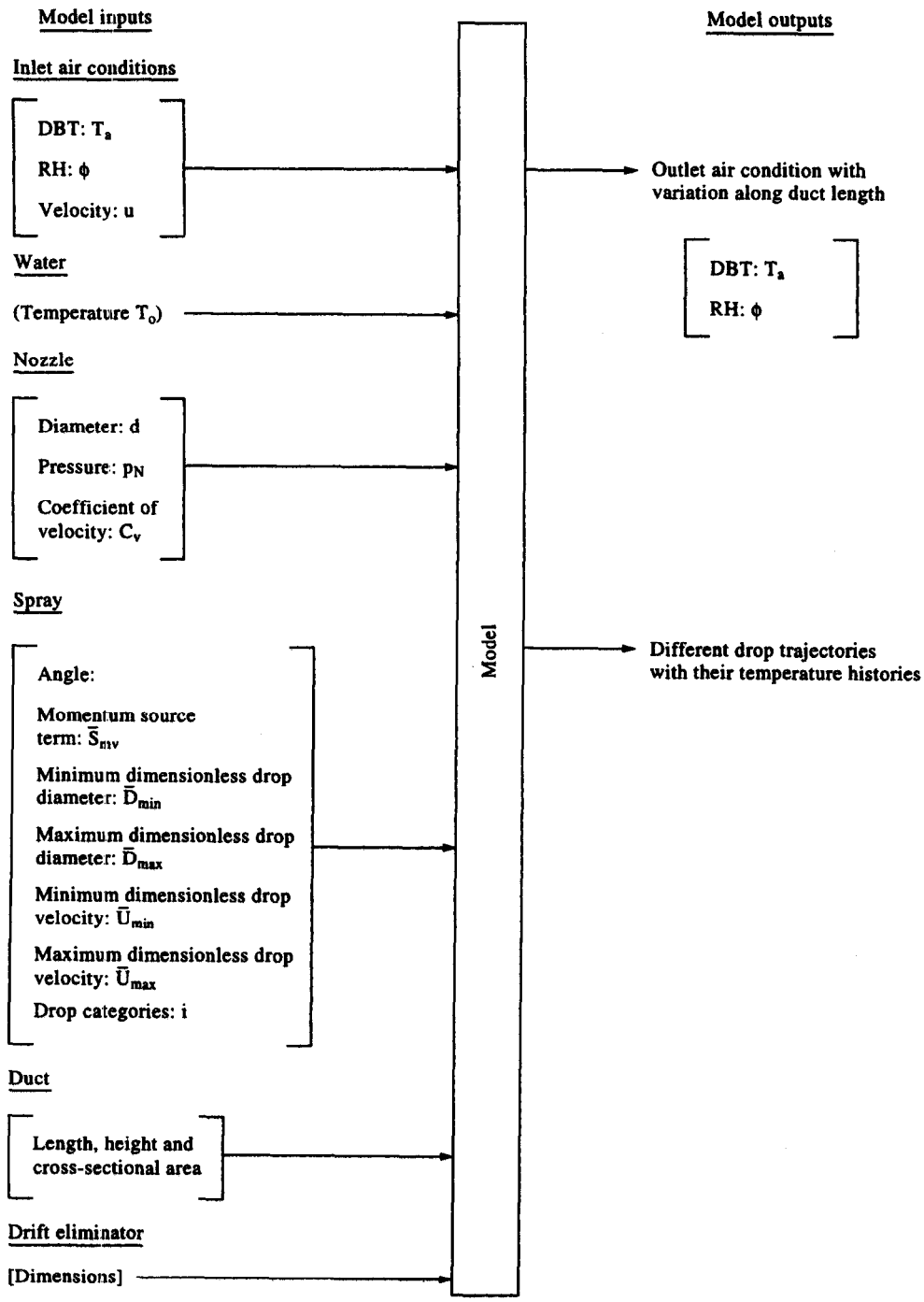

Fig. 3. Overall model inputs and outputs

energy components. The surface energy component, $\bar{S}_e$, is a function of surface area which increases between the nozzle exit and the location of drop formation just downstream of the sheet break-up. The kinetic energy component of $\bar{S}_e$, however, decreases between nozzle exit and break-up. Thus, overall there is negligible energy transfer between the water and surroundings and, hence, the energy source term, $\bar{S}_e$, is taken to be zero. The momentum source term, $\bar{S}_{mv}$, is estimated by calculating the drag force on the sheet cone portion of the hollow cone spray. The cone experiences slip velocity with the air on its outer and inner surface whose magnitude is approximately equal to the nozzle velocity. For simplifying the calculations, the sheet cone is considered as a flat triangular sheet experiencing an air flow of velocity U_0 (Fig. 5). For this configuration, the coefficient of friction C_f is greater than or equal to 0.01 on the outside surface of

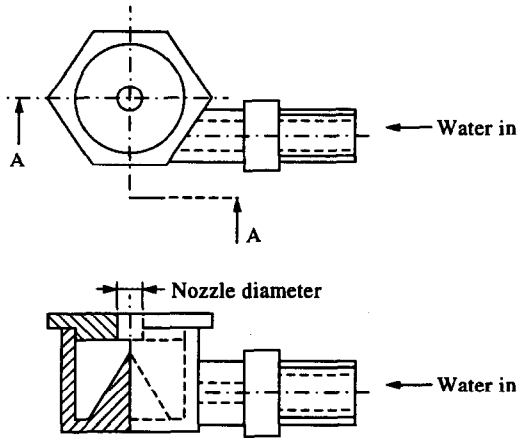

Fig. 4. Nozzle geometry.

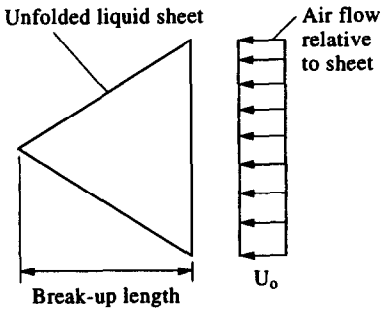

Fig. 5. Model for calculating drag force on the sheet cone region.

the cone. For zero external air velocity, vortical structures are formed inside the cone due to which, the sheet cone inside experiences negligible velocity gradient. Drag on the inside surface is neglected due to this reason [27]. Using drag on one surface, the magnitude of $\bar{S}_{mv}$ is about 0.01. With this value, difficulties were encountered in the MEP formulation and, hence, during computation the value of $\bar{S}_{mv}$ was taken as -0.03 (negative sign signifying loss of momentum) in all the cases. Physically, it means that there is a 3% momentum loss of the spray sheet between nozzle exit and break-up plane. Negligible variation in the shape of the drop distribution curve was observed with ± 0.01 change in $\bar{S}_{mv}$.

The experiments indicated that the values of the non-dimensional drop diameter, i.e. drop diameter normalized by volume mean diameter ($\bar{D}_{30}$), varied from 0 to 2.5. These values were taken as model inputs for $\bar{D}_{min}$ and $\bar{D}_{max}$, respectively. The final MEP model inputs are the upper and lower values of the non-dimensional velocities, $\bar{U}_{max}$ and $\bar{U}_{min}$, respectively. These values were taken from literature as 1.5 and 0.5, respectively. Using these inputs, the constants a_0, a_1, a_2 and a_3 in the MEP formulation were calculated [34] and an explicit joint drop size and velocity distribution function was obtained.

This joint drop size-velocity distribution function was separately integrated over non-dimensional diameter range of 0–0.5, 0.5–1.0, 1.0–1.5, 1.5–2.0 and 2.0–2.5 over non-dimensional velocity range 0.5–1.5. This integration yields the number fraction of drops for five values of dimensionless diameter, namely, 0.25, 0.75, 1.25, 1.75 and 2.25. Dimensionless mean velocities for these dimensionless diameters were calculated from the joint distribution function by dividing the non-dimensional velocity range (0.5–1.5) into 10 zones with an increment of 0.1. The available average velocities for these zones are 0.55, 0.65, ..., 1.45. The dimensionless mean velocity for the non-dimensional diameter range of 0–0.5, for which the average diameter value is 0.25, is calculated as follows:

$$\bar{U}_{\text{mean,1}} = \frac{0.55\int_0^{0.5}\int_{0.5}^{0.6} f\,d\bar{U}\,d\bar{D} + 0.65\int_0^{0.5}\int_{0.6}^{0.7} f\,d\bar{U}\,d\bar{D} + \ldots + 1.45\int_0^{0.5}\int_{1.4}^{1.5} f\,d\bar{U}\,d\bar{D}}{\int_0^{0.5}\int_{0.5}^{1.5} f\,d\bar{U}\,d\bar{D}}. \quad (32)$$

Similarly, the dimensionless mean velocities for other dimensionless diameter zones were calculated. Figure 6 shows a typical result for 3.2 mm diameter nozzle drop size distribution function.

These number fractions were used for computing the number of drops in each size range by multiplying corresponding number fraction by the total number of drops produced at break-up. The latter has been calculated by the following relation:

$$N = \frac{6Q_{act}}{\pi D_{30}^3}. \quad (33)$$

The combination of experimental measurements and MEP formalism were used in this manner to obtain the number of drops and their mean velocities at break-up for the hollow cone water spray in quiescent ambient air. This data were input for the heat and mass transfer simulation.

4.2. *Heat and mass transfer experiments*

The spray nozzle was positioned co-linear with the centre line of a square wind tunnel for heat and mass transfer studies. A schematic diagram of the experimental facility is shown in Fig. 7.

4.2.1. *Wind tunnel facility.* (a) *Air system*: Ambient air is sucked by an adjustable speed blower into a 1.2×1.2 m cross-section conditioning section, via a diffuser. The former consists of a settling chamber followed by a honeycomb, screens, a second settling

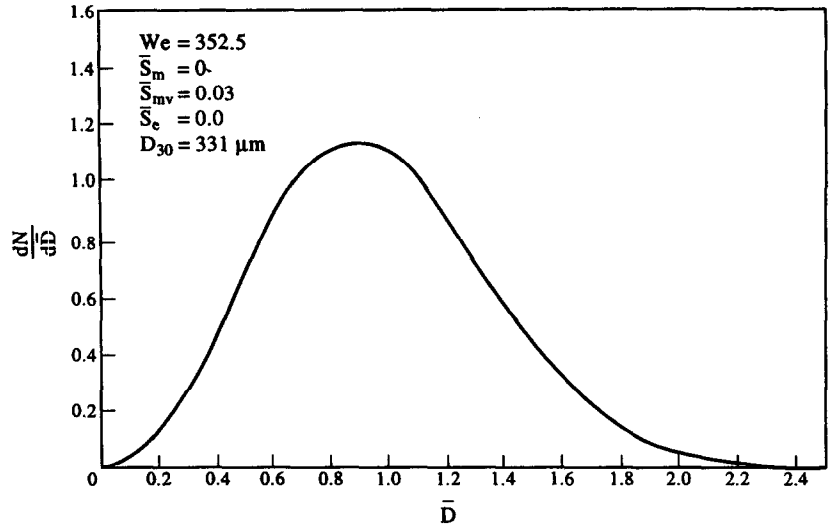

Fig. 6. Number based drop size distribution curve for 3.2 mm diameter nozzle at a pressure of 1 bar(g).

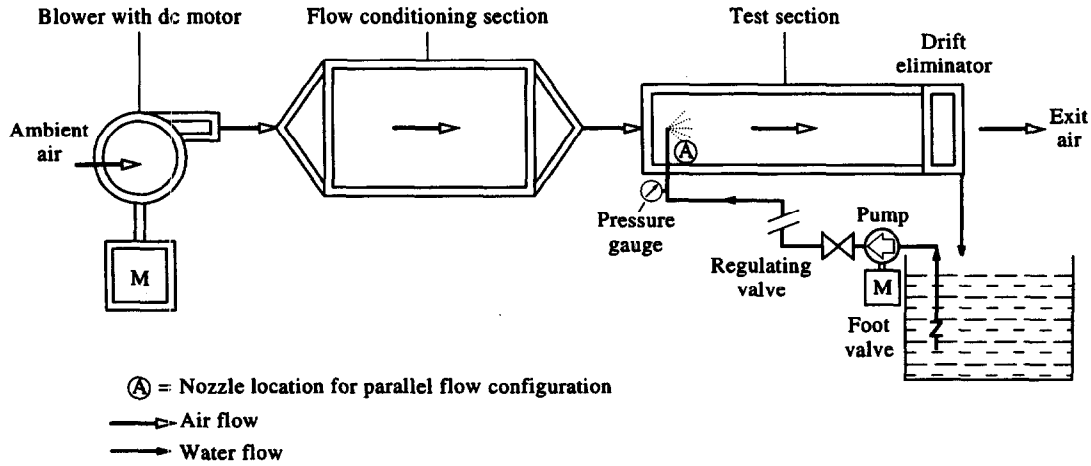

Fig. 7. Schematic diagram of wind-tunnel facility.

chamber, honeycomb, and a contraction cone. The screens consist of a series of fine wire meshes which ensure that large scale eddies are removed at the expense of the introduction of a large number of eddies of much smaller scale which decay in the downstream settling chamber. After flowing through the second settling chamber, the air passes through a 4 : 1 nozzle and enters the perspex test section, 0.6×0.6 m. In this test section, one spray nozzle arranged in parallel flow configuration relative to the air flow gives a nozzle density of 2.8 per square metre which is typical of commercial air washeries and spray cooling systems. The test section is inclined downwards in the air flow direction for draining off the water and a drift eliminator consisting of several parallel plates, each bent twice at right angles and spaced 36 mm apart, was located at the test section exit. It was at this exit plane where air velocity and outlet conditions were measured.

(b) *Water system*: A schematic of the water spray system is shown in Fig. 7. Tank water was pumped through a control valve into the nozzle. The nozzle pipe was mounted vertically from the tunnel top, at the joint between the wind tunnel contraction cone and test section for parallel flow. The nozzle outlet orifice was oriented along the centre line of the test section cross-section. The water drops fall to the bottom of the test section from were the water flows into the tank. To quantify the temperature rise across the pump, separate experiments were conducted for measuring the water temperature in the tank and at the nozzle using thermocouples. Air velocity was measured at the exit of the drift eliminator with a hand held anemometer equipped with a digital readout whose range was 0.2 to 40 m/s with a resolution of 0.1 m/s. The inlet air temperature and relative humidity were measured with a pair of shielded RTDs, one of which was kept moist by a wick dipped in a jar of

water. The range and resolution of the RTD were 0 to 100 and 0.1°C, respectively.

4.2.2. *Experimental procedure.* The once-through design of the wind tunnel necessitated experimentation during the months of April, May and June when Delhi climate is characterized by high ambient temperature, and low relative humidity and capable of significant evaporative cooling. Two sets of experiments were performed in May and June 1993 (Set I) and June, 1995 (Set II). Ambient conditions varied from 35 to 42°C DBT and 22–60% relative humidity. Ambient water temperature during these months was in the range of 26–33°C.

The experiments were first conducted with the 3.2 mm diameter nozzle. At each setting of pressure, measurements were performed at three air velocities namely, 0.8, 1.6 and 2.5 m/s. At each air velocity, the measurements were performed at three pressures 1, 2 and 3 bar(g).

For each run, the velocity was measured at nine locations across the drift eliminator face, one at each corner, at the centre of each side and one at the centre of exit face (Fig. 8). The average of these values was used for adjusting the blower speed to obtain preselected values. Immediately, thereafter, the DBT and relative humidity were measured at these same nine locations. These measurements enabled characterization of the spatial variations across duct cross-section caused by the square duct axisymmetric spray combination and also due to the influence of gravity which may be expected to cause greater cooling in the lower half of the duct relative to the upper half. Velocity variations across the face were ± 0.1 to ± 0.25 m/s which is comparable to the anemometer resolution. The velocity distribution across the face and, hence, tunnel cross-section can, therefore, be considered to be uniform. As there was no control over the RH and DBT of the ambient air supplied by the blower, therefore, these were measured at the outlet of the test section at the beginning of each observation with the spray shut-off. The total time for nine readings of each run was about 40 min during which ambient condition changes were found to be insignificant. Tank water temperature was measured thrice during each run and its average was used to characterize the inlet water temperature of drops. After experimentation with the 3.2 mm diameter nozzle, the same procedure was repeated with the 4.8 mm diameter nozzle with the same set of nozzle pressures and air velocities.

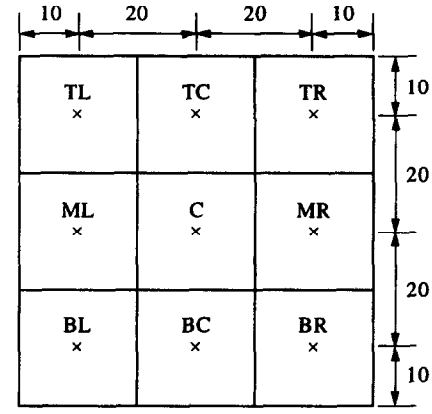

Fig. 8. Measurement location at the exit plane of the drift eliminator.

4.3. *Experimental uncertainties*

For a meaningful comparison of experimental data with model predictions, it is necessary to quantify the uncertainties in the measurements of ambient DBT and RH, outlet DBT and RH, spray pressure and air velocity. The vane type anemometer accuracy was $\pm$ (2% + one digit) which results in uncertainty values between ± 14.5 to ± 5.3% for velocities from 0.8 to 3.0 m/s, the range of air velocities used in the experiments. The response time of the anemometer was about 30 s which was the time required for each measurement and about 4 min for a set of nine readings. The resolution of the DBT and relative humidity measurements was limited by the instrument readout to ± 0.1°C and ± 1%, respectively. However, it is important to note that uncertainty in relative humidity is governed by the uncertainty in WBT which was measured by the RTD moistened by a wick, and also by the absolute values of DBT and WBT. Thus, at conditions of 42°C DBT and 25% relative humidity, the ± 0.1°C uncertainty in each of these measurements, results in an absolute relative humidity uncertainty of about ± 1%. However, at 30°C DBT and 90% relative humidity, similar uncertainties of ± 0.1°C in each measurement results in uncertainties of up to ± 3%, which are greater than the readout resolution. On the basis of the above, ambient DBT and relative humidity have uncertainties of ± 0.1°C and ± 1%, respectively. The maximum uncertainties in exit DBT and relative humidity measurements are ± 0.1°C and ± 3%, respectively.

The response time for this type of RTD (SS shielded) is about 120 s, and when used for measuring the WBT, it is expected to be higher. Measurements indicated that steady values were attained after about 4 min. The ambient temperature and relative humidity for each run were measured at the beginning after which about 40–45 min were required for recording the air velocity, DBT and RH at nine exit locations. During this time, it is possible that the ambient conditions could change, thus introducing an uncertainty in the ambient DBT and RH. From the measurements of ambient conditions, it was observed that during this time interval maximum change in DBT was ± 0.5°C and in relative humidity up to ± 5%. The runs have, therefore, been characterized by DBT and RH at the start of the experiment with individual

uncertainties of ±0.5°C and ±5% (absolute variation), respectively. The nine measurements across the exit face of the wind tunnel showed variations in DBT and RH of up to ±0.5°C and ±16% (absolute variation) about the mean which has been considered as the outlet condition for the particular run. Variations of DBT and RH between upper and lower half are ±1.0°C and ±10% about their individual mean values, respectively.

5. RESULTS AND DISCUSSION

5.1. *Experimental results*

The results of experiments on the wind tunnel setup are summarized in Fig. 9. For each nozzle, DBT and humidity ratio changes from inlet to exit for different water pressures are shown. It is seen that for constant air velocity, the air DBT change increases with nozzle pressure. This trend is expected since with increase in nozzle pressure, water flow rate increases and simultaneously the mean drop diameter decreases. Both these changes increase the area of contact between the drops and air thereby increasing both heat and mass transfer between air and water. For the same reasons the change in air DBT is greater with the 4.8 mm diameter nozzle as compared to 3.2 mm diameter nozzle, for given air velocity–water pressure combination.

Figure 9(a) shows that DBT change at a given air velocity for either nozzle does not follow the same trend. The effect of increasing air velocity on DBT change for a given nozzle diameter-pressure combination is also seen in Fig. 9(a). In general, it is expected that for fixed air intake conditions and water temperature, DBT change will decrease with increasing air velocity. This behaviour can be attributed to the increased mass flow rate of air which causes a relatively smaller change in DBT. There are, however, exceptions to this trend in some cases. This behaviour arises due to the fact that DBT change is strongly influenced by air inlet conditions and water temperature, other parameters being constant. These parameters could not be controlled in the experiment and, hence, the data has not been collapsed by using non-dimensional parameters. Correlations have, therefore, not been proposed either. These complex changes can be studied further by using the model developed.

Figure 9(b) shows that in most cases, the humidity ratio change increases with increasing pressure at constant air velocity. These trends are to be expected for the same reasons as for DBT changes given in the preceding paragraph. Similarly, in general, for a given nozzle pressure, the humidity ratio change is expected to decrease with increasing air velocity. This trend is unambiguously seen for the 4.8 mm diameter nozzle, but for the 3.2 mm nozzle the trend is not so clear.

The relative trends in both DBT and humidity ratio changes are more clearly discernable for the 4.8 mm diameter nozzle as compared to the 3.2 mm diameter nozzle, in spite of comparable change in air inlet DBT

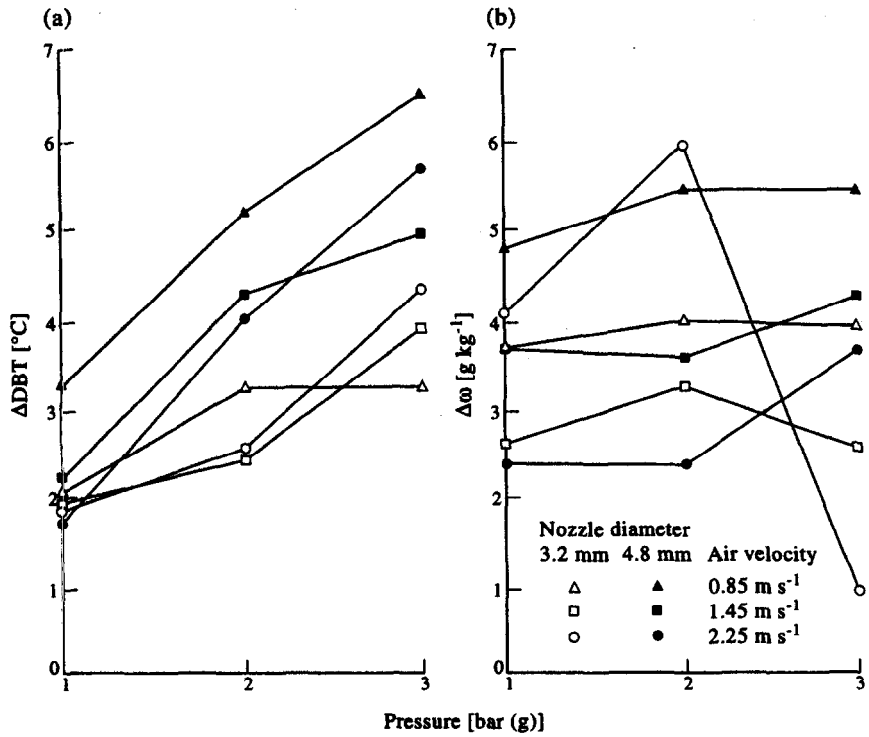

Fig. 9. Change in DBT and humidity ratio with nozzle pressure.

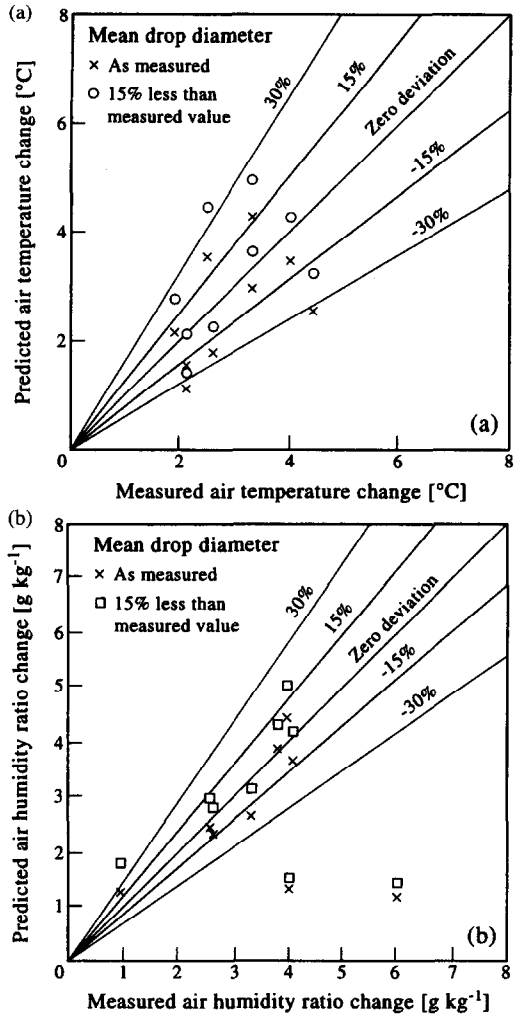

Fig. 10. (a) Comparison of experimental data and model predictions of air temperature (DBT) change for 3.2 mm nozzle diameter; (b) comparison of experimental data and model predictions of air humidity ratio change for 3.2 mm nozzle diameter.

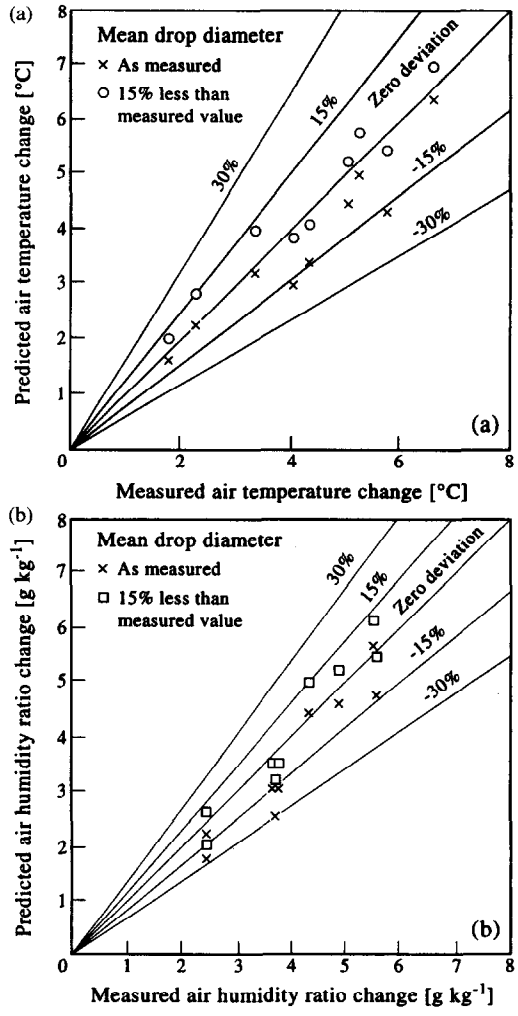

Fig. 11. (a) Comparison of experimental data and model predictions of air temperature (DBT) change for 4.8 mm nozzle diameter; (b) comparison of experimental data and model predictions of air humidity ratio change of 4.8 mm nozzle diameter.

and RH, and in water temperature. This behaviour is primarily a result of the nozzle characteristics where mass flow rate changes with pressure are relatively high for 4.8 mm diameter nozzle whereas the same are not so significant for the 3.2 mm diameter nozzle. The mass flow rate at a given pressure increases with nozzle diameter and Fig. 10 shows this aspect by the relatively greater values of DBT and RH changes for 4.8 mm diameter nozzle in comparison to the 3.2 mm diameter nozzle.

5.2. *Simulation results and comparison with experimental data*

The simulation results using the model (Section 3.3) are given in Figs 10 and 11 for 3.2 and 4.8 mm diameter nozzles, respectively. In Figs 10 and 11 two sets of outlet DBT-RH pairs are given, one using the actual volume mean drop diameter and the other using a mean drop diameter 15% smaller than this value. In each case the drop diameter distribution functions were obtained individually. Such an exercise was necessitated by the fact that actual drop diameter generally underpredicted changes in DBT and humidity ratio. This aspect for 3.2 and 4.8 mm diameter nozzles is shown in Figs 10 and 11, respectively, where measured and predicted changes in DBT and changes in humidity ratio have been plotted. The 45° line in this figure indicates perfect prediction of experimental values and two sets of lines representing ± 15 and $\pm 30\%$ match are also shown. Reasons for these underpredictions were explored in detail and are given below.

Simulations were performed with four mean drop diameters, 15 and 30% greater, 15 and 30% less than measured mean drop diameter. Large mean diameter further underpredicted the changes and were not investigated further. The best match was obtained with a diameter 15% smaller than the mean drop

diameter relative to 30% smaller diameter. For these reasons the detailed results with 15% reduction in drop diameter are presented.

This observation points towards the possibility that actual mean drop sizes during experiments may have been smaller than the measured values. Such a possibility can be attributed to two reasons. Firstly, drop size measurements were performed in a still environment, whereas in wind tunnel experiments the spray is formed in a dynamic air medium. Due to the interaction of spray sheet and forced air movement, as against induced air flow due to the spray [16], drop size could decrease. Comprehensive mathematical analyses of this kind of interaction for subject nozzles are not available in literature. Forced air flow affects the drop trajectories which could cause secondary break-up of drops due to collisions. Secondly, the photographic method used to measure drop size is unable to capture small diameter drops, less than 65 μm. The photographs are thus biased towards larger drop sizes and result in an increase in measured volume mean diameter. Due to limitations in experimental facilities, this aspect could not be explored further. The use of a laser based technique could yield better resolution of drop diameter distribution. This equipment was, however, not available. Therefore, after considering the above-mentioned possibilities, it was decided to examine the effect of a reduction in mean drop size on prediction of outlet air conditions, without varying other experimental parameters. Comparison of measured outlet air condition with model predictions based on actual drop size and 15% decrease in drop size, reveals that in majority of observations, measured air condition values fall within the bound of these two predicted values. Graphical interpretation of these results are shown in Figs 10 and 11.

Changes in predicted air temperature and humidity ratio are plotted against experimental values for 3.2 mm diameter nozzle in Figs 10(a) and (b), respectively. In Fig. 10(a), six out of nine data of predicted air temperature change, based on actual drop size prediction are below zero deviation line. With a 15% decrease in drop size, predicted data are uniformly distributed on both sides of the zero deviation line. Except one, all the predicted air temperature data based on 15% decrease in drop size fall within the bound of $\pm 30\%$ deviation. Figure 10(b) shows predicted air humidity ratio change as compared with the measured values. In this case also, a majority of predictions based on actual drop size are either on or below the mean line. With a 15% reduction in drop size, a majority of predicted data are above the zero deviation line. Two-thirds of the data of predicted humidity ratio change (based on 15% decrease in drop size) lie between -15 and $+30\%$ uncertainty limit.

For the 4.8 mm diameter nozzle, predictions for air temperature change and humidity ratio change are given in Figs 11(a) and (b), respectively. All predictions of air temperature change, based on actual drop size are between 0 and -30% deviation line. Predictions corresponding to 15% decrease in drop size are distributed within $\pm 15\%$ deviation. Trends of predicted air humidity ratio change [Fig. 11(b)] are similar to Fig. 10(b). Here, also, it can be concluded that predictions of humidity ratio change (based on 15% decrease in drop diameter) for 4.8 mm diameter are within a close limit of $\pm 15\%$.

Actual model predictions for DBT and humidity ratio change (with respect to nozzle pressure for constant air velocity) for 4.8 mm diameter nozzle are relatively consistent with experimental data than 3.2 mm diameter nozzle. With the 4.8 mm diameter nozzle, overall predictions corresponding to 15% decrease in drop size are relatively more accurate as compared to those for the 3.2 mm diameter nozzle. This uncertainty increase is attributed to the low water flow rate due to which overall magnitude of measured air DBT and humidity ratio change are small for the 3.2 mm diameter nozzle as compared to the 4.8 mm diameter nozzle. This increases the errors due to uncertainties in experimental measurements. Irrespective of nozzle size, the magnitude of prediction changes (both for air DBT and humidity ratio) below or above 4 g/kg or 4°C can be predicted satisfactorily within ± 30 and $\pm 15\%$, respectively. In industrial air washer systems, typical DBT change is greater than 4°C. Therefore, for DBT changes greater than this value, predictions can be made with an accuracy of $\pm 15\%$ for either nozzle diameter.

Due to experimental difficulties in measuring DBT and RH in the duct during spray operation, it is not possible to obtain this data on property variations within the duct. This data, important for optimizing duct length, can be obtained from the model and a representative case is discussed below.

Figure 12 shows the prediction of DBT and humidity ratio (for 15% decrease in drop diameter) along duct length where, the air velocity is 1.5 m/s, nozzle pressure 2 bar(g) and nozzle diameter 4.8 mm. Air inlet condition is 37°C DBT and 54% relative humidity (humidity ratio 24.9 g/kg). Up to 0.4 m downstream distance, the DBT decreases linearly (about 4°C/m) and humidity ratio also increases linearly (about 6.0 g/kg/m). The change after 0.4 m distance is also linear, but less rapid as can be seen by the sudden change in slope at 0.4 m distance. The reason for this behaviour is seen in the drop trajectories shown in Fig. 13, where drops of diameter 290, 406 and 522 μm hit the duct wall and are thus removed from the computation. 174 μm diameter drops which originate with downward trajectories also exhibit similar behaviour. Such an abrupt removal of drops is not expected in reality, due to the continuous nature of drop diameter distribution. In reality, the removal of drops due to contact with the walls occurs over a finite distance depending upon their diameter. The trajectories of other drops continue downstream into the duct and continue to effect the heat and mass transfer. In this case, typical of parallel flow, the entire

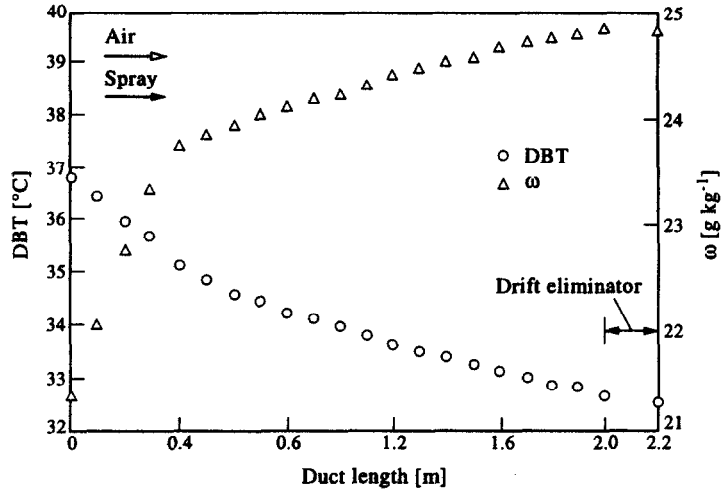

Fig. 12. DBT and humidity ratio variations along the duct for horizontal parallel flow [nozzle diameter 4.8 mm, pressure 2.0 bar(g)].

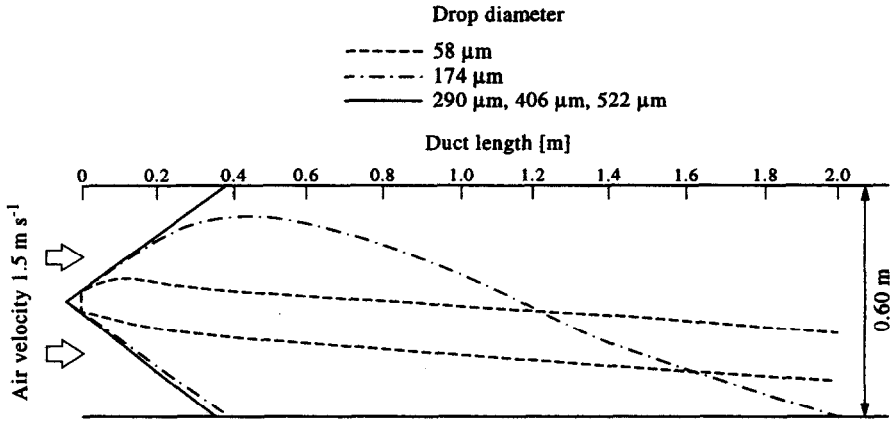

Fig. 13. Drop trajectories in the duct for horizontal parallel flow [nozzle diameter 4.8 mm, pressure 2.0 bar(g)].

duct length contributes towards evaporative cooling. The relative contribution of the first 20% length is about 40% of the cooling effect because all drops are involved in the heat transfer. Thus, for enhancing cooling effect, the drop–air interaction length needs to be increased, which can be realized by delaying drop collisions with the wall. This objective can be attained by using a spray of smaller angle with a given duct.

5.3. *Sensitivity analysis of model predictions*

The models for drop diameter prediction and heat and mass transfer computations require several input parameters, some of which are estimated and others measured experimentally. With each parameter, there is an associated uncertainty. This uncertainty produces corresponding uncertainty in the model predictions. This sensitivity to input condition variations is described below. Sensitivity of model predictions to variations in mean drop diameter have already been discussed elsewhere and are not repeated here.

5.3.1. *Coefficient of velocity.* In the modelling of the spray, the coefficient of velocity for the nozzle is required for calculating the nozzle exit velocity [equation (32)]. For the nozzles used, this parameter is not available and, therefore, had to be estimated. Flow through an orifice most closely approximates flow through the nozzle. The coefficient of velocity for orifices are typically between 0.85 and 0.95 and a value of 0.9 was used in the calculations. This ± 0.05 absolute variation in the value of C_v, results in variations in the model predictions. For a typical case, DBT and humidity ratio changes vary by a maximum of ± 0.1°C and 0.2 g/kg, respectively.

5.3.2. *Water temperature.* The variation of water temperature during a run was ± 0.6°C. Apart from this value there is uncertainty due to temperature rise measurement across the pump which was measured by thermocouples and a millivoltmeter. The combined uncertainty due to instrument limitations and repeatability during experiments is 0.2°C. In the model, the water temperature was perturbed by ± 2°C for given air inlet conditions, nozzle pressure and drop size distribution. The resultant variations in outlet DBT and

humidity ratio changes were ± 0.5°C and ± 0.8 g/kg, respectively.

5.3.3. *Inlet air conditions.* The measurement uncertainties in inlet air DBT, and WBT, are ± 0.5°C [Section 4.3], which together result in $\pm 5\%$ variation in relative humidity (3 g/kg variations in humidity ratio). This perturbation of ± 0.5°C in DBT, for fixed WBT, results in an uncertainty in relative humidity ratio simultaneously. Alternatively, variation with constant relative humidity produces a change in WBT. For given inlet air relative humidity, air velocity, water pressure and water temperature a variation of ± 1°C in inlet air DBT produced changes of ± 0.8°C in exit air DBT and a humidity ratio change of 1.2 g/kg.

5.3.4. *Model sensitivities.* The above data shows that, the dominating uncertainty in model predictions results from uncertainties in mean drop diameter. For this reason, comparisons of model output and experimental measurements have been performed for variations in mean drop diameter only.

6. CONCLUSIONS

The main objective of the present research was to develop a simple and efficient numerical model for estimation of heat and mass transfer between water spray drops and an air stream in horizontal parallel flow configuration to enable accurate prediction of evaporative cooling performance. The major findings of this research are summarized below.

(a) Joint drop diameter and velocity distribution function for hollow cone water sprays can be determined using still photography data in conjunction with the MEP formalism.
(b) Experiments indicate that DBT decrease of up to 9°C is attainable by employing evaporative cooling during dry summer months.
(c) A heat and mass transfer model for simulating the conservation equations has been developed with discrete drop diameters which uses drop data from the MEP formalism. The model was used for simulating drop dynamics in two-dimensions and one-dimensional heat and mass transfer between drops and air for horizontal parallel flow configuration. The predictions are within $\pm 15\%$. The code could be used for designing industrial evaporative cooling systems.

REFERENCES

1. Masters, K., *Spray Drying Handbook*, 4th edn. Wiley, New York, 1991.
2. Yeung, W. S., Dynamics of gas liquid spray systems. In *Encyclopedia of Fluid Mechanics*, Vol. 3, Chapter 12, 1986, pp. 281–300.
3. Crowe, C. T., Sharma, M. P. and Stock, D. E., The particle source-in-cell (PSI-CELL) model for gas droplet flows. *ASME Journal of Fluids Engineering*, 1977, **99,** 325–352.
4. Harlow, F. M. and Amsden, A. A., Numerical calculation of multiphase fluid flow. *Journal of Computational Physics*, 1975, **17,** 19–52.
5. Hiestand, J. W., Henry, J. M. and Farajian, S., A simple numerical model of a water spray humidifier. ISA-paper #90-11580198-0092/90/1601-1607, 1990.
6. Kachhwaha, S. S., Kale, S. R. and Dhar, P. L., Study of drop size distribution and mass transfer from a hollow cone water spray, Paper no. HMT-94-099. *Proceedings of the First ISHMT—ASME Heat and Mass Transfer Conference*, Bhabha Atomic Research Centre, Bombay, India, 1994, pp. 679–684.
7. Kachhwaha, S. S., Dhar, P. L. and Kale, S. R., Two-dimensional simulation of water spray and air interaction in parallel flow configuration, Paper no. HMT-94-076. *Proceedings of the Second ISHMT—ASME Heat and Mass Transfer Conference*, Karnatak Regional Engineering College, Suratkal, Karnataka, India, 1995, pp. 541–546.
8. Yeung, W. S., Similarity analysis of gas liquid spray systems. *Transactions of the ASME Journal of Applied Mechanics*, 1982, **49,** 687–690.
9. Mawhinny, J. R., Dlugogorski, B. Z. and Kim, A. K., Closer look at the fire extinguishing properties of water mist. *Fire Safety Science—Proceedings of the Fourth International Symposium*, 1994, pp. 47–60.
10. Mohiuddin, A. K. M. and Kant, K., Analysis of mechanical draft water cooling towers. *Journal of Energy, Heat and Mass Transfer*, 1991, **13,** 165–187.
11. Palaszewski, S. J., Jiji, L. M. and Weinbaum, S., A three-dimensional air vapour droplet interaction model. *Journal of Heat Transfer*, 1981, **103,** 514–521.
12. Palaszewski, S. J., Weinbaun, S. and Jiji, L. M., Power plant spray cooling: design and performance studies. *Journal of Engineering Gas Turbine Power*, 1985, **107,** 582–588.
13. Moussiopoulos, N. and Ernst, G., Thermal performances of spray cooling ponds at zero wind velocity. *International Journal of Heat and Mass Transfer*, 1985, **109,** 212–217.
14. Moussiopoulos, N., Numerical simulation of spray cooling pond performance. *Transactions of the ASME: Journal of Fluids Engineering*, 1987, **109,** 179–185.
15. Ghosh, S., and Hunt, J. C. R., Induced air velocity within droplet driven sprays. *Proceedings of the Royal Society of London A*, 1994, **444,** 105–127.
16. Abhishek, Kumar, Fluid dynamics of a hollow cone water spray and air stream, B.Tech. thesis, Mechanical Engineering Department, I.I.T., Delhi, 1994.
17. Ghosh, S. and Hunt, J. C. R., Spray jets in a cross-flow, 1993 (in preparation).
18. Hishida, K., Maeda, M., Imaru, J., Hironaga, K. and Kano, H., Measurement of size and velocity of particles in two-phase flow by a three beam LDA system. In *Laser Anemometry in Fluid Mechanics*, Ladoan-Instituto Superior Technico, Portugal, 1984.
19. Maeda, M., Hishida, K., Sekine, M. and Watanabe, N., Measurement of spray jet using LDV system with particle size discrimination. *Laser Anemometry in Fluid Mechanics—III, 3rd International Symposium on Applications of Laser Anemometry to Fluid Mechanics*, Lisbon, Portugal, 1986.
20. Maeda, M., Sanai, N., Kobashi, K. and Hishida, K., Measurement of spray mist-flow by a compact fiber LDV and Doppler—shift detector with a fast DSP. *Applications of Laser Anemometry to Fluid Mechanics, 4th International Symposium*, Lisbon, Portugal, 1988.
21. Sellens, R. W., Phase Doppler measurements near the nozzle in a low-pressure water spray. *Liquid Particle Size Measurement Techniques*, 2nd Vol., ASTM STP 1083 (eds) E. Dan Hirleman, W. D. Bachalo, and Philip G. Felton, American Society for Testing and Materials, Philadelphia, 1990, pp. 193–208.
22. Li, X., Chin, L. P., Tankin, R. S., Jackson, T., Stutrud,

J. and Switzer, G., Comparison between experiments and predictions based on maximum entropy for sprays from a pressure atomizer. *Combustion Flame*, 1991, **86,** 73–89.
23. Azzopardi, B. J., Measurement of drop sizes. *International Journal of Heat and Mass Transfer*, 1979, **22,** 1245–1279.
24. Natrajan, R., A survey of diagnostic techniques for measurements in liquid sprays. *Experiments in Fluids—Proceedings of the National Symposium*, E. Radhakrishnan, Aerospace Engineering Department, I.I.T., Kanpur, 1992.
25. Mugele, R. A. and Evans, H. D., Droplet size-distribution in sprays. *Industrial and Engineering Chemistry*, 1951, **43**(6), 1317–1324.
26. Lekic, A., Kajramovic, R. and Ford, J. D., Droplet size distribution: an improved method for fitting experimental data. *Canadian Journal of Chemical Engineering*, 1976, **54,** 399–402.
27. Lee, S. Y. and Tankin, R. S., Study of liquid spray (water) in a non-condensable environment (air). *International Journal of Heat and Mass Transfer*, 1984, **27**(3), 351–361.
28. Jaynes, E. T., Information theory and statistical mechanics. *Physics Review*, 1957, **106,** 620–630.
29. Shannon, C. E., *Bell System Technology Journal*, 1948, **27,** 379–423.
30. Kapur, J. N., *Maximum Entropy Models in Science and Engineering*. Wiley Eastern Limited, Delhi, 1989.
31. Kapur, J. N. and Kesavan, H. K., *Entropy Optimization Principles with Applications*. Academic, Boston, 1992.
32. Sellens, R. W. and Brzustowski, T. A., A simplified predictions of droplet velocity distributions in a spray. *Combustion Flame*, 1986, **65,** 273–279.
33. Sellens, R. W., Prediction of drop size and velocity distribution in spray based on the maximum entropy formalism. *Particle and Particle Systems Characterization*, 1989, **6,** 17–27.
34. Li, X. and Tankin, R. S., Derivation of droplet size distribution in sprays by using information theory. *Combustion Science Technology*, 1988, **60,** 345–357.
35. Li, X., Tankin, R. S. and Renksizbulut, M., Calculated characteristics of droplet size and velocity distributions in liquid sprays. *Particle and Particle Systems Characterization*, 1990, **7,** 54–59.
36. Kachhwaha, S. S., Some studies on spray type evaporative cooling process. Ph.D. thesis, Mechanical Engineering Department, I.I.T., Delhi, 1996.
37. Linn, J. D. M., Maskell, S. J. and Patrick, M. A., A note on heat and mass transfer to a spray droplet. *Nuclear Technology*, 1988, **81,** 122–125.
38. Jain, S., Ph.D. thesis, Mechanical Engineering Department, I.I.T., Delhi, 1994.
39. Ranz, W. E. and Marshall, W. R., Evaporation from drops—Part 2. *Chemical Engineering Progress*, 1952, **48,** 173–180.
40. Dewitt, D. P. and Incropera, F. P. *Fundamentals of Heat Transfer*, 3rd edn. Wiley, 1991.
41. Bird, R. B., Stewart, W. E. and Lightfoot, E. N., *Transport Phenomenon*. Wiley, New York, 1960, p. 647.
42. Gnielinski, V., New equations for heat and mass transfer in turbulent pipe and channel flow. *International Chemical Engineering*, 1976, **16,** 359–368.